A COMPUTATIONALLY INEXPENSIVE ALGORITHM FOR DETERMINING OUTER AND INNER ENCLOSURES OF NONLINEAR MAPPINGS OF ELLIPSOIDAL DOMAINS

Andreas Rauh, Luc Jaulin

Int. J. Appl. Math. Comput. Sci., 2021, Vol. 31, No. 3, 399–415
DOI: 10.34768/amcs-2021-0027

A COMPUTATIONALLY INEXPENSIVE ALGORITHM FOR DETERMINING OUTER AND INNER ENCLOSURES OF NONLINEAR MAPPINGS OF ELLIPSOIDAL DOMAINS

ANDREAS RAUH [a,*], LUC JAULIN [a]

[a]Lab-STICC
ENSTA Bretagne
2 rue François Verny, 29806 Brest, France
e-mail: Andreas.Rauh@interval-methods.de, lucjaulin@gmail.com

A wide variety of approaches for set-valued simulation, parameter identification, state estimation as well as reachability, observability and stability analysis for nonlinear discrete-time systems involve the propagation of ellipsoids via nonlinear functions. It is well known that the corresponding image sets usually possess a complex shape and may even be nonconvex despite the convexity of the input data. For that reason, domain splitting procedures are often employed which help to reduce the phenomenon of overestimation that can be traced back to the well-known dependency and wrapping effects of interval analysis. In this paper, we propose a simple, yet efficient scheme for simultaneously determining outer and inner ellipsoidal range enclosures of the solution for the evaluation of multi-dimensional functions if the input domains are themselves described by ellipsoids. The Hausdorff distance between the computed enclosure and the exact solution set reduces at least linearly when decreasing the size of the input domains. In addition to algebraic function evaluations, the proposed technique is—for the first time, to our knowledge—employed for quantifying worst-case errors when extended Kalman filter-like, linearization-based techniques are used for forecasting confidence ellipsoids in a stochastic setting.

Keywords: bounded uncertainty, guaranteed enclosures, ellipsoidal enclosures, inner and outer approximations, nonlinear systems, confidence intervals.

1. Introduction

In the frame of interval analysis (Jaulin *et al.*, 2001; Mayer, 2017), the domains of uncertain variables are commonly described by axis-aligned boxes in a multi-dimensional (state) space $\mathbf{x} \in \mathbb{R}^n$. When applying some nonlinear mapping

$$\mathbf{y} = \mathbf{f}(\mathbf{x}), \quad \mathbf{f}: \mathbb{R}^n \mapsto \mathbb{R}^n \tag{1}$$

to those domains, one typically assumes as well that each component of the resulting image is described independently by a corresponding interval. For that purpose, either all elementary operators (addition, subtraction, multiplication, and division) as well as elementary functions (such as trigonometric, exponential, and logarithmic) are replaced by their interval counterparts using the so-called natural (naive) interval extension.

Due to the fact that this direct replacement of all operators and functions typically leads to conservative bounds due to multiple dependencies on common variables that cannot be accounted for in this kind of evaluation, techniques for a reduction of overestimation using higher-order methods, centered forms, or monotonicity tests are often employed. For an overview about these procedures, the reader is referred to the works of Mayer (2017) and Moore *et al.* (2009).

Using such interval-valued box representations of the solution sets, information about the correlation between the individual vector components y_i, $i \in \{1,\ldots,n\}$, is lost. This is especially critical if iterated function evaluations are performed, for example, in the frame of predictor–corrector approaches for state estimation (Rauh *et al.*, 2021b) or in a simulation-based stability analysis of nonlinear discrete-time systems (Bourgois and Jaulin, 2021), where it is desired to show whether or not some integer value $k > 0$ exists such that the image domain after

*Corresponding author

a k-fold repeated function evaluation leads to a true subset of the initial domain $\mathbf{x} \in \boldsymbol{\mathcal{X}}$. This initial domain $\boldsymbol{\mathcal{X}}$ was assumed as an axis-parallel interval box in the reference above but could be described alternatively by other sets such as ellipsoids, Taylor models, parallelepipeds, zonotopes, or polytopes.

To reduce the pessimism induced by interval wrapping (Jaulin *et al*., 2001), i.e., enclosing the result of the nonlinear function evaluation by an axis-aligned box and propagating this box further in subsequent evaluation steps, several countermeasures were introduced in the literature. Those include domain splitting procedures with subsequent function evaluations for each of the resulting boxes (Rauh *et al*., 2007), the description of solution sets by enhanced shapes such as zonotopes (Kühn, 1999) or high-order Taylor models (Makino and Berz, 2004; Hoefkens, 2001), or the use of an ellipsoidal calculus (Kurzhanskii and Vályi, 1997) employed for state estimation purposes by Becis-Aubry (2020).

However, all of these techniques suffer to at least some extent from an exponential growth of complexity and a curse of dimensionality if subsequent function evaluations are performed in high-dimensional spaces. If domain splitting procedures are concerned, it is often required to perform splitting operations recursively at each evaluation of the nonlinear map $\mathbf{f}(\mathbf{x})$ in (1), where—without merging sufficiently small and similar interval boxes (Rauh *et al*., 2007; Krasnochtanova *et al*., 2010)—the computational complexity inevitably grows in an exponential manner.

Although sensitivity analysis and inner approximations of the solution sets (Goubault *et al*., 2014) may be employed to select the dimension and interval box to be bisected, such information is often ignored for the sake of a simple implementation. Similarly, also for zonotopic enclosures, the complexity increases if successive function evaluations are performed. This is caused by the fact that the number of required vertices typically increases if zonotopic domains are mapped via nonlinear functions. This holds even for linear expressions containing interval parameters. Again, order reduction techniques are required, which are typically only performed heuristically without quantifying the worst-case excess width of each function evaluation. Similar aspects are true for Taylor model arithmetic, where the polynomial orders inevitably grow after each function evaluation. In practice, this growth of the polynomial degrees is countered by absorbing the errors due to a polynomial truncation into interval remainder terms that are often combined with a domain re-scaling.

These complexity issues restrict the successful application to small dimensions n as well as to domains $\boldsymbol{\mathcal{X}}$ that are sufficiently tight. This contradicts the general aim, where it is desired—as is often the case in control engineering—that each evaluation step should

(i) have a closed-form representation of the solution set and

(ii) simultaneously provide computationally cheap information about the worst-case pessimism in terms of the distance between inner and outer enclosures,

regardless of whether or not domain splitting approaches are included in an algorithm.

Here, the second aspect is strongly related to the goal to find a procedure that describes the solution sets by tight enclosures that rapidly converge towards the exact solution if the input domains are reduced in their volume.

In this paper, we propose a novel solution procedure that computes both inner and outer ellipsoidal enclosures of the evaluation of a nonlinear function (1), where the distance between both bounds directly provides a measure for the worst-case excess width. From an application point of view, such (algebraic) function evaluations arise in a large variety of settings. Just to mention a few, these are the evaluation of homogeneous coordinate transformations in robotics which relate joint angles to end-effector coordinates in a Cartesian frame, compute the stationary control effort if an equilibrium configuration is predefined in terms of the joint coordinates, or arise during the prediction of deterministic and stochastic discrete-time system models between two subsequent sampling points. Especially in the latter setting, which to our knowledge has not yet been considered in the literature in the frame of an ellipsoidal calculus, the representation of both inner and outer bounds in terms of ellipsoids provides the information about extremal probability distributions between which a Gaussian approximation of the result may be included.

The existing state-of-the-art approaches for using ellipsoidal set representations, such as the ellipsoidal toolbox developed by Kurzhanskiy and Varaiya (2006), are partially restricted to dominantly linear or polynomial systems. They are commonly based on the solution of linear matrix inequalities (LMIs) in each evaluation step and/or employ computationally expensive min-max optimization approaches with quite a large number of degrees of freedom. Simplifications of these techniques can be obtained by relaxing the employed optimality criteria (typically, replacing logarithmic cost functions by linear ones (cf. Tarbouriech *et al*., 2011)) or by reducing the number of available degrees of freedom, where only a stretch parameter (cf. Rauh *et al*., 2021b) needs to be optimized after the structure of the ellipsoid shape matrix is predefined in advance.

In addition, Taylor model approaches (developing the solutions of ordinary differential equations into high-order series in initial states, parameters, and the

time variable (cf. Bünger, 2020)) can be combined in an efficient way with an ellipsoidal calculus if long-term simulations of dynamic systems are of interest. This has been shown by Villanueva *et al*. (2015) and Houska *et al*. (2015), who employed ellipsoidal enclosures to bound the Taylor models' remainder terms and in such a way replace the classically employed interval bounds for these error terms. Typically, these ellipsoid bounds need to be computed numerically, i.e., without simple closed-form expressions such as those presented in this paper.

On the one hand, the methods developed by Villanueva *et al*. (2015) and Houska *et al*. (2015) have the advantage to be more precise than interval-based approaches due to the use of higher-order Taylor models. On the other hand, however, the increased computational effort is only beneficial if evaluations of dynamic systems over long time spans are desired. For single function evaluations, over sufficiently tight domains, as well as for the embedding into predictor–corrector type state estimators, the approaches quoted above are less suited due to two properties. First, the ellipsoidal bounds proposed in the quoted papers are based on the solution of some auxiliary system models, which may be prohibitive for real-time application in state estimation for systems with fast dynamics. Second, intersections of computed state bounds with set-valued representations of measured data as performed by Rauh *et al*. (2021b) typically destroy the advantage of Taylor models of representing complexly shaped solution domains for dynamic systems with smooth dynamics.

Due to these reasons, we develop closed-form inner and outer ellipsoidal enclosures in this paper which do not require the solution of any auxiliary system model. Note that, in this paper, we restrict ourselves to the evaluation of static system models given in the explicit form (1) and to applications in the frame of discretized system models. The use in continuous-time settings will be the subject of future work, where the case of temporarily varying uncertain parameters will be of interest. This latter aspect renders high-order series expansions inappropriate because bounds for a finite number of time derivatives of the uncertain parameters are typically not available if such kinds of differential inclusions are investigated.

This paper is structured as follows. Section 2 gives an overview of related solution ideas, before the actual solution approach is derived in Section 3. Illustrating examples are given in Sections 4 and 5, where the former deals with the mapping of ellipsoidal domains via nonlinear functions and the latter is focused on applying the proposed technique to forecasting specific confidence ranges for system models with stochastic uncertainty. Finally, an outlook on further possible applications and research concludes this paper in Section 6.

2. Problem formulation and related solutions

Assume that the initial domain $\mathbf{x} \in \mathcal{X}$ is described by the quadratic form

$$\mathcal{E}_x := \left\{ \mathbf{x} \in \mathbb{R}^n \;\middle|\; (\mathbf{x}-\boldsymbol{\mu}_x)^T \boldsymbol{\Gamma}_x^{-T} \boldsymbol{\Gamma}_x^{-1} (\mathbf{x}-\boldsymbol{\mu}_x) \leq 1 \right\} \quad (2)$$

representing a nondegenerate ellipsoid with the positive definite shape matrix $\boldsymbol{\Gamma}_x \boldsymbol{\Gamma}_x^T \succ 0$ and the midpoint $\boldsymbol{\mu}_x \in \mathbb{R}^n$. The final goal is to find a computationally simple procedure so that the range $\mathbf{y}$ of the function values is included in an ellipsoid $\mathcal{E}_y$.

In contrast, a straightforward evaluation of the range of a nonlinear function according to (1) over the ellipsoid $\mathcal{E}_x$ can be described either by a centered form representation of the nonlinear map or by using a linear Taylor model approach. In the first case, a suitable interval extension of the Jacobian[1]

$$\frac{\partial \mathbf{f}}{\partial \mathbf{x}}(\mathbf{x}) \in [\mathbf{J}_\mathbf{f}] \quad (3)$$

is required for a tight interval box $[\mathbf{x}] \supset \mathcal{E}_x$. As already stated in Introduction, the interval extension in (3) is typically obtained by replacing all mathematical operations included in the Jacobian $\frac{\partial \mathbf{f}}{\partial \mathbf{x}}(\mathbf{x})$ by their respective interval counterparts.[2] Using the set value membership (3), the range of $\mathbf{y}$ can be bounded by

$$\left\{ \begin{array}{l} \mathbf{y} = \mathbf{f}(\mathbf{x}) \\ \mathbf{x} \in \mathcal{E}_x \end{array} \right. \quad \Longrightarrow \quad \left\{ \begin{array}{l} \mathbf{y} = \mathbf{f}(\boldsymbol{\mu}_x) + \mathbf{J}_\mathbf{f} \cdot (\mathbf{x}-\boldsymbol{\mu}_x) \\ \mathbf{J}_\mathbf{f} \in [\mathbf{J}_\mathbf{f}] \,. \end{array} \right. \quad (4)$$

If $[\mathbf{J}_\mathbf{f}]$ only contains strictly nonsingular realizations of the Jacobian, $\mathbf{x} = \boldsymbol{\mu}_x + \mathbf{J}_\mathbf{f}^{-1} \cdot (\mathbf{y} - \mathbf{f}(\mathbf{x}))$ can be substituted into the ellipsoid definition (2).

The result then is the convex hull over ellipsoids with interval-valued shape matrices and uncertain (box-constrained) midpoints. If a simple-shape representation of the result in terms of a single ellipsoid with a point-valued midpoint is desired, two steps are required that can be solved by using LMI techniques, namely, finding a tight ellipsoidal enclosure over the union of the continuum of ellipsoids with uncertain shape matrices and, then, enclosing its Minkowski sum (de Berg

[1] As an alternative to computing the Jacobian by means of algorithmic or symbolic differentiation, the corresponding slope matrix could be used (Griewank, 2000; Chapoutot, 2010).

[2] Since the algorithm presented in the following section only needs the evaluation of Jacobian matrices for interval boxes and avoids the direct interval evaluation of the function (1), the corresponding arguments are defined by a tight axis-aligned box containing the ellipsoid $\mathcal{E}_x$; see also Fig. 1. Further tightening the enclosures would only be possible by higher-order derivatives (e.g., a centered form representation of the Jacobian which would lead to the necessity to compute the function's Hessian) for a description of the ranges for $\mathbf{x}$ in a rotated coordinate frame which requires symbolic reformulations of the Jacobian to reduce overestimation. Such approaches are not considered further to keep the algorithm as simple as possible.

et al., 2008) with a hyper-rectangle by solving a further optimization problem. Although this approach is computationally feasible and can be implemented by means of the ideas from Jambawalikar and Kumar (2008), Halder (2018), and Yildirim (2006), the solution of LMIs generates a non-negligible computational effort that should be avoided within this paper to obtain a fast closed-form solution. Note that these LMI-based approaches essentially make use of the findings by John (1948) and Černý (2012), who showed how a tight outer bounding ellipsoid (the so-called Löwner–John ellipsoid) can be found which describes a convex hull over a cloud of individual points in a multi-dimensional space.

An alternative to the enclosure (4) of the range of $\mathbf{y}$ is the use of the linear Taylor model of the nonlinear map given by

$$\mathbf{y} \in \left[\mathbf{b}'\right] + \mathbf{A}' \cdot (\mathbf{x} - \boldsymbol{\mu}_x) \quad \text{with} \quad \mathbf{x} \in \mathcal{E}_x, \tag{5}$$

where $\mathbf{A}'$ is a strictly regular, real-valued point matrix and $[\mathbf{b}']$ is an interval vector that is chosen so that all function values of (1) over the domain of interest are guaranteed to be included in the right-hand side expression of (5). Although, in contrast to (4), this approach avoids the necessity of finding the union over ellipsoids with uncertain shape matrices, the problem of finding an ellipsoid close to the Minkowski sum of an ellipsoid and a hyper-rectangle still exists.

Due to the simplified nature of (5) in comparison with (4), this formulation is used as the basis for the derivation of a procedure for a linear change of coordinates with which the aforementioned Minkowski sum can be evaluated exactly as the sum of the radii of two concentric balls.

Notation. Throughout this paper, $\|\cdot\|$ represents the Euclidean norm of the corresponding vector-valued argument. In the cases where the argument is an n-dimensional interval vector $[\mathbf{x}]$, an interval-valued generalization of the norm is defined as

$$\|[\mathbf{x}]\| = \sqrt{\sum_{i=1}^{n} [x_i]^2}, \tag{6}$$

where the infima of $[x_i]^2$ and $\|[\mathbf{x}]\|$ are nonnegative. For more general (ellipsoidal) arguments, it is defined as the supremum over all possible Euclidean norms that can be overapproximated conservatively by means of suitable interval bounds of the argument.

3. Ellipsoidal enclosures

Theorem 1. (Outer ellipsoidal enclosure) *Define the non-degenerate ellipsoid*

$$\mathcal{E}_x := \left\{ \mathbf{x} \in \mathbb{R}^n \;\middle|\; (\mathbf{x} - \boldsymbol{\mu}_x)^T \boldsymbol{\Gamma}_x^{-T} \boldsymbol{\Gamma}_x^{-1} (\mathbf{x} - \boldsymbol{\mu}_x) \le 1 \right\}. \tag{7}$$

For a differentiable function $\mathbf{y} = \mathbf{f}(\mathbf{x})$, $\mathbf{f} : \mathbb{R}^n \mapsto \mathbb{R}^n$, *with*

$$\mathbf{A} = \frac{\partial \mathbf{f}}{\partial \mathbf{x}} (\boldsymbol{\mu}_x) \quad \textit{invertible}, \tag{8}$$

$$\mathcal{E}_y^{\mathrm{O}} := \left\{ \mathbf{y} \in \mathbb{R}^n \;\middle|\; (\mathbf{y} - \boldsymbol{\mu}_y)^T \boldsymbol{\Gamma}_{y,\mathrm{O}}^{-T} \boldsymbol{\Gamma}_{y,\mathrm{O}}^{-1} (\mathbf{y} - \boldsymbol{\mu}_y) \le 1 \right\} \tag{9}$$

is an outer enclosure of the solution set $\mathbf{f}(\mathcal{E}_x)$ *with*

$$\boldsymbol{\mu}_y = \mathbf{f}(\boldsymbol{\mu}_x) \quad \textit{and} \quad \boldsymbol{\Gamma}_{y,\mathrm{O}} = (1+\rho) \cdot \mathbf{A} \cdot \boldsymbol{\Gamma}_x, \tag{10}$$

where

$$\rho = \max_{\|\tilde{\mathbf{x}}\| \le 1} \left\| \tilde{\mathbf{b}}(\tilde{\mathbf{x}}) \right\|, \tag{11}$$

and

$$\tilde{\mathbf{b}}(\tilde{\mathbf{x}}) = \boldsymbol{\Gamma}_x^{-1} \cdot \mathbf{A}^{-1} \cdot \Big(\mathbf{f}(\boldsymbol{\Gamma}_x \tilde{\mathbf{x}} + \boldsymbol{\mu}_x) - \mathbf{f}(\boldsymbol{\mu}_x) \Big) - \tilde{\mathbf{x}}. \tag{12}$$

Proof. First, set

$$\tilde{\mathbf{x}} = \boldsymbol{\Gamma}_x^{-1} \cdot (\mathbf{x} - \boldsymbol{\mu}_x). \tag{13}$$

From (7), we have

$$\tilde{\mathbf{x}} \in \mathcal{S}_x := \left\{ \tilde{\mathbf{x}} \;\middle|\; \|\tilde{\mathbf{x}}\| \le 1 \right\}. \tag{14}$$

Second, define

$$\tilde{\mathbf{y}} = \tilde{\mathbf{x}} + \tilde{\mathbf{b}}(\tilde{\mathbf{x}}), \tag{15}$$

which represents $\mathbf{y}$ after applying the linear change of coordinates (13) with $\tilde{\mathbf{b}}(\tilde{\mathbf{x}})$ given in (12). Hence, according to the triangle inequality,

$$\|\tilde{\mathbf{y}}\| \le \|\tilde{\mathbf{x}}\| + \left\|\tilde{\mathbf{b}}(\tilde{\mathbf{x}})\right\| = 1 + \rho \tag{16}$$

holds with

$$\rho = \min_{\rho \in \mathbb{R}^+} \left\{ \rho \in \mathbb{R}^+ \;\middle|\; \left\|\tilde{\mathbf{b}}(\tilde{\mathbf{x}})\right\| \le \rho \;,\; \forall \tilde{\mathbf{x}} \in \mathcal{S}_x \right\}. \tag{17}$$

Alternatively, (15) can be expressed as $\tilde{\mathbf{y}} \in \mathcal{S}_x \oplus \mathcal{S}_b$, where $\oplus$ is the Minkowski sum of two sets (de Berg *et al.*, 2008) and

$$\tilde{\mathbf{b}}(\tilde{\mathbf{x}}) \in \mathcal{S}_b := \{ \tilde{\mathbf{x}} \mid \|\tilde{\mathbf{x}}\| \le \rho \}. \tag{18}$$

Therefore, $\tilde{\mathbf{y}}$ belongs to a ball of radius $1+\rho$ as illustrated in Fig. 1. According to (12) and (15), the equality

$$\tilde{\mathbf{y}} = \boldsymbol{\Gamma}_x^{-1} \cdot \mathbf{A}^{-1} \cdot (\mathbf{y} - \boldsymbol{\mu}_y) \tag{19}$$

holds. Substituting this equality into (16) yields the ellipsoid $\mathcal{E}_y^{\mathrm{O}}$ according to (9)–(10), which completes the proof. ■

Remark 1. For sufficiently small domains $\mathcal{E}_x$, $\left\|\tilde{\mathbf{b}}(\tilde{\mathbf{x}})\right\| \to 0$ uniformly holds and implies that the ellipsoid $\mathcal{E}_y^{\mathrm{O}}$ becomes an arbitrarily tight outer enclosure of $\mathbf{f}(\mathcal{E}_x)$ according to the following theorem. In contrast to the Löwner–John ellipsoids (cf. John, 1948; Černý, 2012), however, the proposed bounds are not necessarily the tightest possible, i.e., minimal enclosures.

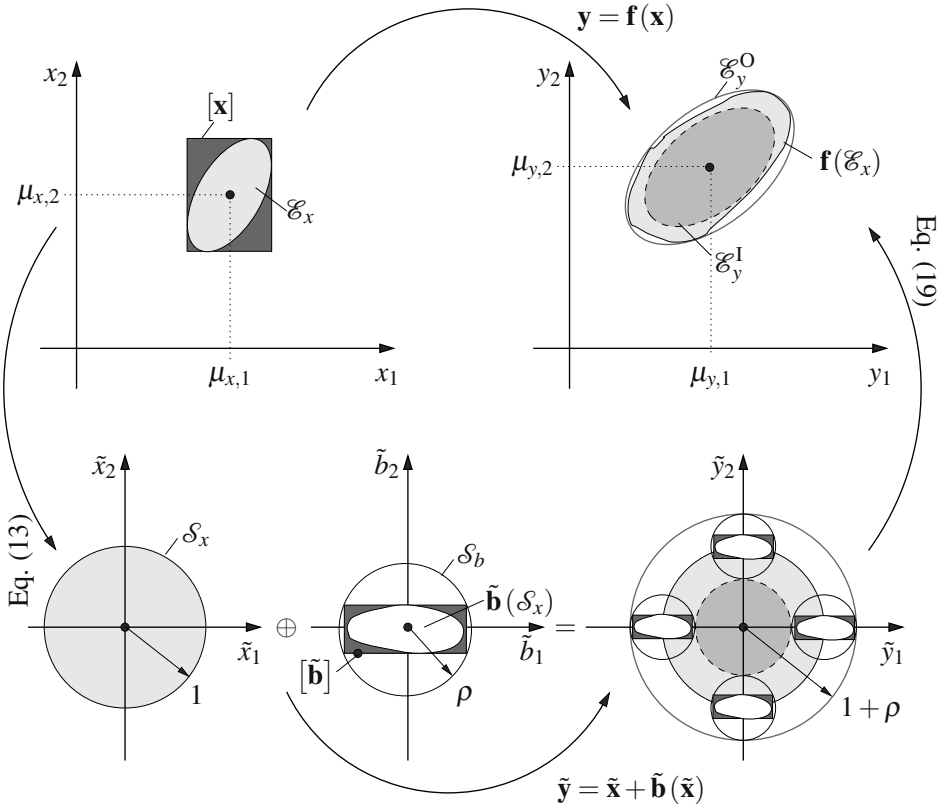

Fig. 1. Ellipsoidal enclosure approach. As visualized above, the domain $\tilde{\mathbf{b}}(\mathcal{S}_x)$ becomes close to an ellipsoid or a ball if the domain $\mathscr{E}_x$ is sufficiently small.

Theorem 2. (Asymptotic convergence of the enclosure $\mathscr{E}_y^{\mathrm{O}}$) *The parameter ρ defined in Theorem 1 is a measure for the maximum deviation between $\mathscr{E}_y^{\mathrm{O}}$ and the true set $\mathbf{f}(\mathscr{E}_x)$. The Hausdorff distance between $\mathbf{f}(\mathscr{E}_x)$ and the ellipsoid $\mathbf{y} \in \mathscr{E}_y^{\mathrm{O}}$ is of order $o(\|\mathbf{x} - \boldsymbol{\mu}_x\|)$. Equivalently, this also implies $\rho \to 0$, as stated in the remark above.*

Proof. The difference between the exact solution set $\mathbf{f}(\mathscr{E}_x)$ and its ellipsoidal enclosure $\mathbf{y} \in \mathscr{E}_y^{\mathrm{O}}$ is proportional to $\tilde{\mathbf{b}}(\tilde{\mathbf{x}})$. Differentiability of the map $\mathbf{f}$ implies the existence of a Lipschitz constant $\tilde{L} > 0$ as

$$\|\mathbf{f}(\mathscr{E}_x) - \mathbf{y}\| \leq \tilde{L} \cdot \|\tilde{\mathbf{x}}\| \tag{20}$$

and, therefore, also

$$\|\mathbf{f}(\mathscr{E}_x) - \mathbf{y}\| \leq L \cdot \|\mathbf{x} - \boldsymbol{\mu}_x\|, \tag{21}$$

with $L > 0$. Hence, for decreasing domain sizes $\mathscr{E}_x$, the ellipsoid $\mathscr{E}_y^{\mathrm{O}}$ converges at least linearly to the true result. ■

Theorem 3. (Inner ellipsoidal enclosure) *An inner ellipsoidal approximation of the solution set $\mathbf{f}(\mathscr{E}_x)$ is given by*

$$\mathscr{E}_y^{\mathrm{I}} := \left\{ \mathbf{y} \in \mathbb{R}^n \;\middle|\; (\mathbf{y} - \boldsymbol{\mu}_y)^T \boldsymbol{\Gamma}_{y,\mathrm{I}}^{-T} \boldsymbol{\Gamma}_{y,\mathrm{I}}^{-1} (\mathbf{y} - \boldsymbol{\mu}_y) \leq 1 \right\} \tag{22}$$

with

$$\boldsymbol{\mu}_y = \mathbf{f}(\boldsymbol{\mu}_x) \quad \textit{and} \quad \boldsymbol{\Gamma}_{y,\mathrm{I}} = (1-\rho) \cdot \mathbf{A} \cdot \boldsymbol{\Gamma}_x, \tag{23}$$

where $\mathbf{A}$ and ρ are defined in Theorem 1.

Proof. Following the same steps as in the proof of Theorem 1, a domain belonging to the image set for all possible $\tilde{\mathbf{x}} \in \mathcal{S}_x$ is obtained by evaluating the Minkowski difference

$$\mathcal{S}^{\mathrm{I}} = \mathcal{S}_x \ominus \mathcal{S}_b. \tag{24}$$

For $\rho \in [0\,;\,1]$, the ball with a maximum volume fully inscribed in this domain $\mathcal{S}^{\mathrm{I}}$ has the radius $1 - \rho$. According to Eqn. (19), this gives the inner ellipsoid $\mathscr{E}_y^{\mathrm{I}}$ in (22)–(23). ■

Remark 2. For $\rho > 1$, the inner enclosure is the empty set.

A computationally feasible implementation of the ellipsoidal outer and inner enclosures is summarized in Algorithm 1. It directly implements the solution approach proposed in Theorems 1 and 3. To solve the optimization task given in Eqn. (11), an interval arithmetic approach is utilized to find a tight upper bound for the parameter ρ by determining the upper interval bound (supremum) of the

Algorithm 1. Outer and inner ellipsoidal enclosures.

Input: $\mathbf{f}(\mathbf{x})$, $\{\boldsymbol{\mu}_x, \boldsymbol{\Gamma}_x\}$
Output: $\{\boldsymbol{\mu}_y, \boldsymbol{\Gamma}_{y,\mathrm{O}}, \boldsymbol{\Gamma}_{y,\mathrm{I}}\}$

1: $[x_i] = \mu_{x,i} + \|\boldsymbol{\Gamma}_{x,i}\| \cdot [-1\ ;\ 1]\ ,\ \ i \in \{1,\ldots,n\}$
2: $[\mathbf{x}] = [x_1] \times \ldots \times [x_n]$
3: $\mathbf{A} = \frac{\partial \mathbf{f}}{\partial \mathbf{x}}(\boldsymbol{\mu}_x)$
4: $\boldsymbol{\Gamma}_y = \mathbf{A} \cdot \boldsymbol{\Gamma}_x$
5: $[\mathbf{J_f}] = \left[\frac{\partial \mathbf{f}}{\partial \mathbf{x}}\right]([\mathbf{x}])$
6: $\left[\tilde{\mathbf{b}}\right] = \left(\boldsymbol{\Gamma}_y^{-1} \cdot [\mathbf{J_f}] \cdot \boldsymbol{\Gamma}_x - \mathbf{I}\right) \cdot [-1\ ;\ 1]_{\times n}$
7: $\rho = \sup\left\{\left\|\left[\tilde{\mathbf{b}}\right]\right\|\right\}$
8: $\boldsymbol{\mu}_y = \mathbf{f}(\boldsymbol{\mu}_x)$
9: $\boldsymbol{\Gamma}_{y,\mathrm{O}} = (1+\rho) \cdot \boldsymbol{\Gamma}_y$
10: $\boldsymbol{\Gamma}_{y,\mathrm{I}} = (1-\rho) \cdot \boldsymbol{\Gamma}_y$

Euclidean norm of the vector $\left[\tilde{\mathbf{b}}\right]$ as

$$\rho \leq \sup\left\{\left\|\left[\tilde{\mathbf{b}}\right]\right\|\right\}, \tag{25}$$

with

$$\tilde{\mathbf{b}}(\tilde{\mathbf{x}}) \in \left[\tilde{\mathbf{b}}\right] := \left(\boldsymbol{\Gamma}_x^{-1} \cdot \mathbf{A}^{-1} \cdot [\mathbf{J_f}] \cdot \boldsymbol{\Gamma}_x - \mathbf{I}\right) \cdot [\tilde{\mathbf{x}}]. \tag{26}$$

Here, we make use of a centered form (mean value form) representation of $\left[\tilde{\mathbf{b}}\right]$ according to

$$\left[\tilde{\mathbf{b}}\right] = \tilde{\mathbf{b}}(\tilde{\mathbf{x}}_0) + \left[\frac{\partial \tilde{\mathbf{b}}}{\partial \tilde{\mathbf{x}}}\right]([\tilde{\mathbf{x}}]) \cdot ([\tilde{\mathbf{x}}] - \tilde{\mathbf{x}}_0), \tag{27}$$

where $\tilde{\mathbf{x}}_0 = \mathbf{0}$ and $\tilde{\mathbf{b}}(\mathbf{0}) = \mathbf{0}$. To reduce overestimation due to the wrapping effect of interval analysis as far as possible, the involved Jacobian $\frac{\partial \tilde{\mathbf{b}}}{\partial \tilde{\mathbf{x}}}$ is expressed along with

$$\frac{\partial \mathbf{f}}{\partial \tilde{\mathbf{x}}}(\tilde{\mathbf{x}}) = \frac{\partial \mathbf{f}}{\partial \mathbf{x}}(\mathbf{x}) \cdot \frac{\partial \mathbf{x}}{\partial \tilde{\mathbf{x}}}(\tilde{\mathbf{x}}) = \frac{\partial \mathbf{f}}{\partial \mathbf{x}}(\mathbf{x}) \cdot \boldsymbol{\Gamma}_x \in [\mathbf{J_f}] \cdot \boldsymbol{\Gamma}_x, \tag{28}$$

where $[\mathbf{J_f}]$ is an interval extension of $\frac{\partial \mathbf{f}}{\partial \mathbf{x}}$ (cf. (3)), over the tightest axis-aligned box $[\mathbf{x}]$ in original coordinates which contains the ellipsoid $\mathscr{E}_x$.

This box, sketched in Fig. 1, is determined by finding those points of the ellipsoid $\mathscr{E}_x$ that have an outward directed normal vector that is parallel to the i-th unit vector $\mathbf{e}_i$, $\|\mathbf{e}_i\| = 1$, of $\mathbb{R}^n$ and is then projected onto the i-th axis. The corresponding computation of these points $\mathbf{x}_i^*$ is given by the collinearity condition

$$\nabla \mathscr{E}_x \propto \boldsymbol{\Gamma}_x^{-T} \boldsymbol{\Gamma}_x^{-1} \cdot (\mathbf{x}_i^* - \boldsymbol{\mu}_x) = \alpha \mathbf{e}_i \tag{29}$$

for the normal vector $\nabla \mathscr{E}_x$, which yields

$$\boldsymbol{\Gamma}_x^{-1} \cdot (\mathbf{x}_i^* - \boldsymbol{\mu}_x) = \alpha \boldsymbol{\Gamma}_x^T \mathbf{e}_i. \tag{30}$$

Choosing

$$\alpha = \frac{1}{\left\|\boldsymbol{\Gamma}_x^T \mathbf{e}_i\right\|} \tag{31}$$

so that the condition

$$\left\|\boldsymbol{\Gamma}_x^{-1} \cdot (\mathbf{x}_i^* - \boldsymbol{\mu}_x)\right\| = \alpha \left\|\boldsymbol{\Gamma}_x^T \mathbf{e}_i\right\| = 1 \tag{32}$$

is satisfied implies that $\mathbf{x}_i^*$ lies on the ellipsoid surface.

Hence, with $\boldsymbol{\Gamma}_x^T = \boldsymbol{\Gamma}_x$, line 1 of Algorithm 1 is verified according to

$$x_i^* - \mu_{x,i} = \mathbf{e}_i^T \cdot (\mathbf{x}_i^* - \boldsymbol{\mu}_x) = \left\|\boldsymbol{\Gamma}_x^T \mathbf{e}_i\right\| = \|\boldsymbol{\Gamma}_x \mathbf{e}_i\| = \|\boldsymbol{\Gamma}_{x,i}\|, \tag{33}$$

where $\boldsymbol{\Gamma}_{x,i}$ is the i-th column of $\boldsymbol{\Gamma}_x$.

Remark 3. The advantage of the centered form representation of $\left[\tilde{\mathbf{b}}\right]$ in (26) over directly replacing all function evaluations by corresponding interval counterparts using naive interval extensions is the reduction of overestimation which decreases at least quadratically for a reduction of the width of the interval $[\mathbf{x}]$. This general property of the centered form evaluation was observed and proved by Moore (1966) as well as Cornelius and Lohner (1984). In the approach considered, this property holds if $\mathbf{A}^{-1} \cdot [\mathbf{J_f}]$ in (26) is sufficiently close to a point-valued identity matrix. If this is not the case, a direct evaluation of (12) may be advantageous; see also the work of Tóth and Csendes (2005).

Remark 4. Because lines 3, 4, and 8–10 of Algorithm 1 are evaluated in floating-point arithmetic, possible round-off errors resulting from the use of a finite-precision arithmetic are currently neglected in the implementation. However, they can be captured rigorously by evaluating the corresponding lines of the algorithm using verified methods including outward rounding which automatically leads to suitably increasing the value of the parameter ρ. However, in most engineering applications, this effect can be neglected to reduce computing times. In state estimation tasks, such as those presented in Rauh *et al.* (2021b), the major contributions to the value of ρ are uncertain parameters, bounded disturbances, and the size of the domain $\mathscr{E}_x$ itself.

4. Example 1: Mapping of ellipsoidal domains

In this section, several examples for general as well as volume-preserving nonlinear function evaluations $\mathbf{y} = \mathbf{f}(\mathbf{x})$ are given. All of them stem from the area of discretized dynamic systems, so that the notation $\mathbf{x}_{k+1} = \mathbf{f}(\mathbf{x}_k)$ is used in the following.

4.1. General nonlinear function evaluation. As a first benchmark application for the proposed ellipsoidal

enclosure approach, consider the nonlinear function

$$\mathbf{x}_{k+1} = \mathbf{f}(\mathbf{x}_k) = \begin{bmatrix} x_{1,k} \\ x_{2,k} \\ x_{3,k} \end{bmatrix} + 0.2 \cdot \begin{bmatrix} 1 + x_{1,k}^2 x_{2,k} - 2.5 x_{1,k} + 0.5 x_{3,k}^2 \\ 1.5 x_{1,k} - x_{1,k}^2 x_{2,k} \\ -0.5 x_{3,k}^2 \end{bmatrix} \tag{34}$$

inspired by a one time step explicit Euler discretization of the two-dimensional Brusselator model according to Goubault *et al*. (2014) and Bouissou *et al*. (2013), which has been extended by a third state variable $x_{3,k}$. The Brusselator is a simple dynamic system representing oscillatory dynamics in chemical reactions.[3] From this perspective, the added term $x_{3,k}$ describes a temporally varying external disturbance influencing the nonlinear dynamics.

Throughout this subsection, it is assumed that $\mathcal{E}_{x,k}$ is given by a ball $\left\|\mathbf{x}_k - \boldsymbol{\mu}_{x,k}\right\| \leq R$, $\boldsymbol{\Gamma}_{x,k} = R \cdot \mathbf{I}$, with the radius $R > 0$ and the midpoint $\boldsymbol{\mu}_{x,k} = \begin{bmatrix} 1 & 1.5 & 0.5 \end{bmatrix}^T$.

In Table 1, the parameter ρ and the volumes of the inner and outer ellipsoidal enclosures ($\mathrm{vol}\left\{\mathcal{E}^{\mathrm{I}}_{x,k+1}\right\}$ and $\mathrm{vol}\left\{\mathcal{E}^{\mathrm{O}}_{x,k+1}\right\}$, resp.) are compared together with the rate of reduction in ρ in comparison with its value ρ^* that is obtained for the radius $R = 1$. To obtain a conservative comparison, ρ and $\mathrm{vol}\left\{\mathcal{E}^{\mathrm{O}}_{x,k+1}\right\}$ are rounded upwards, all other data are rounded downwards to the number of displayed digits.

Firstly, it can be noticed that the maximum overestimation of the ellipsoidal enclosure reduces for decreasing sizes of the domains $\mathcal{E}_{x,k}$. As shown in Theorem 2, the Hausdorff distance between the true image of the nonlinear map and the ellipsoidal enclosure decreases at least linearly with the domain width. This is confirmed by computing the ratio between ρ and its value for the largest initial domain under consideration; see also Fig. 2 for a visualization on a double logarithmic scale. Moreover, as soon as an inner enclosure exists according to Theorem 3, the distance between $\mathcal{E}^{\mathrm{I}}_{x,k+1}$ and $\mathcal{E}^{\mathrm{O}}_{x,k+1}$ reduces rapidly for a decreasing size of $\mathcal{E}_{x,k}$.

This property is also shown graphically in Fig. 3, where the left column contains a comparison of the verified outer enclosure with a grid-based approximation of the nonlinear map, while the right one shows a comparison of the inner ellipsoid (gray shaded surface) and the outer one (black mesh) for two values of R.

4.2. Volume-preserving maps. To perform a fair comparison between natural interval extensions of nonlinear functions and the proposed ellipsoidal evaluation approach for higher-dimensional system models, two volume-preserving maps are considered in this subsection.

[3] A Python implementation of this example as well as a further 2-dimensional benchmark are available for download at `https://www.ensta-bretagne.fr/jaulin/ellipse.html`.

Table 1. Influence of the ball radius R on the pessimism of the ellipsoidal enclosures with $\rho^* = \rho(R = 1)$.

R	ρ	ρ^*/ρ	$\mathrm{vol}\left\{\mathcal{E}^{\mathrm{I}}_{x,k+1}\right\}$	$\mathrm{vol}\left\{\mathcal{E}^{\mathrm{O}}_{x,k+1}\right\}$
2^0	3.540	1.000	–	331.50
2^{-1}	1.570	2.255	–	7.516
2^{-2}	0.735	4.815	0.001	0.290
2^{-4}	0.175	20.29	$4.86 \cdot 10^{-4}$	0.0015
2^{-6}	0.044	82.26	$1.18 \cdot 10^{-5}$	$1.54 \cdot 10^{-5}$
2^{-8}	0.011	330.1	$2.04 \cdot 10^{-7}$	$2.19 \cdot 10^{-7}$

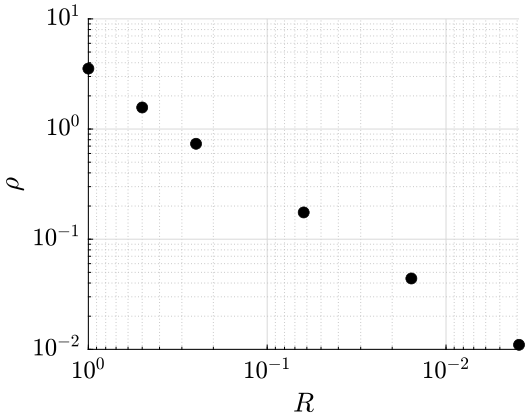

Fig. 2. Reduction of ρ for a decreasing ball radius R.

4.2.1. Dubins car model. The first example in this subsection is a Dubins car model (Romig *et al*., 2019)

$$\mathbf{x}_{k+1} = \mathbf{f}(\mathbf{x}_k) = \begin{bmatrix} x_{1,k} \\ x_{2,k} \\ x_{3,k} \\ x_{4,k} \end{bmatrix} + T \cdot \begin{bmatrix} \cos\left(x_{4,k}\right) \cdot x_{3,k} \\ \sin\left(x_{4,k}\right) \cdot x_{3,k} \\ 0 \\ 0 \end{bmatrix} \tag{35}$$

that is discretized with the help of an explicit Euler method (step size $T = 1$). This model includes an uncertainty in its temporally constant orientation $x_{4,k}$. This angle of orientation is included in the state equations in terms of a discrete-time integrator disturbance model as the fourth state variable. The other states are the positions $x_{1,k}$ and $x_{2,k}$ as well as the absolute value of the car's constant, but uncertain velocity $x_{3,k}$. As initial conditions for the ellipsoidal evaluation approach, the states $\mathbf{x}_k$ are assumed to be included in an ellipsoid $\mathcal{E}_{x,k}$ with the center

$$\boldsymbol{\mu}_{x,k} = \begin{bmatrix} 1 & 1 & 0.1 & \frac{\pi}{3} \end{bmatrix}^T \tag{36}$$

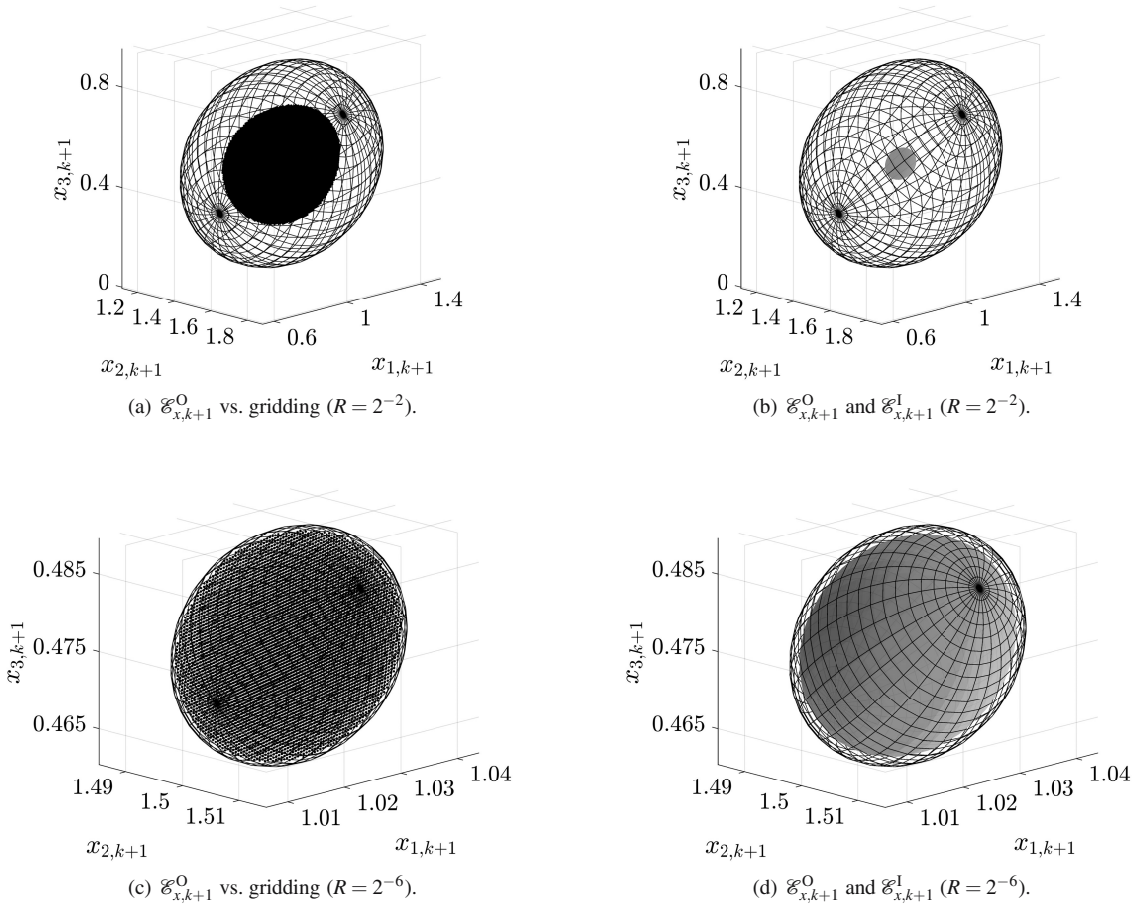

(a) $\mathscr{E}^{\mathrm{O}}_{x,k+1}$ vs. gridding ($R = 2^{-2}$).

(b) $\mathscr{E}^{\mathrm{O}}_{x,k+1}$ and $\mathscr{E}^{\mathrm{I}}_{x,k+1}$ ($R = 2^{-2}$).

(c) $\mathscr{E}^{\mathrm{O}}_{x,k+1}$ vs. gridding ($R = 2^{-6}$).

(d) $\mathscr{E}^{\mathrm{O}}_{x,k+1}$ and $\mathscr{E}^{\mathrm{I}}_{x,k+1}$ ($R = 2^{-6}$).

Fig. 3. Comparison of $\mathscr{E}^{\mathrm{O}}_{x,k+1}$ and $\mathscr{E}^{\mathrm{I}}_{x,k+1}$ for different values of R.

and the diagonal shape matrix

$$\mathbf{C}_{x,k} = \begin{bmatrix} 0.01 & 0 & 0 & 0 \\ 0 & 0.01 & 0 & 0 \\ 0 & 0 & R^2 & 0 \\ 0 & 0 & 0 & R^2 \end{bmatrix}. \tag{37}$$

The alternative, interval-based function evaluation makes use of a tight axis-aligned box $[\mathbf{x}_k]$ enclosing this ellipsoid according to Eqns. (29)–(33).

Table 2 summarizes the results for the evaluation of this model for both alternative techniques, in terms of the parameter ρ of the ellipsoidal enclosure, the ratio $\mathrm{vol}\left\{\mathscr{E}^{\mathrm{O}}_{x,k+1}\right\}/\mathrm{vol}\left\{\mathscr{E}^{\mathrm{I}}_{x,k+1}\right\}$ between outer and inner ellipsoid volumes in the step $k+1$, a comparison of the volumes $\mathrm{vol}\left\{\mathscr{E}^{\mathrm{O}}_{x,k+1}\right\}/\mathrm{vol}\left\{\mathscr{E}_{x,k}\right\}$, and finally the ratio $\mathrm{vol}\{[\mathbf{x}_{k+1}]\}/\mathrm{vol}\{[\mathbf{x}_k]\}$ of the volumes of a classical interval evaluation applied directly to the system model (35). It can be seen that the parameter ρ reduces rapidly for decreasing parameters $R > 0$. This decrease is an indicator for the reduction of the excess width between inner and outer ellipsoid bounds. If the last two columns of this table are compared, it can be seen that the interval (box-type) evaluation may produce less overestimation for large domains, for which the inner ellipsoid bound is empty. However, a decrease in the initial domain size leads to a rapid improvement of the ellipsoidal enclosures, which is mainly due to the fact that the wrapping effect (Jaulin *et al.*, 2001) of interval analysis becomes less important for mappings that are close to a linear one (for sufficiently small domains) if the regions of interest are described by ellipsoids and not naively by boxes. It should be pointed out that this quality improvement is indicated directly by parameters ρ becoming sufficiently close to zero, while such a quantification is not directly possible in a classical interval extension of (35).

For small domains, the ellipsoidal evaluation then directly maps an ellipsoid to an ellipsoid, while the interval counterpart inevitably becomes more pessimistic due to the wrapping effect. Note that the change of coordinates indicated in Fig. 1 would allow reducing overestimation in the interval case by implementing affine

Table 2. Comparison of the ellipsoidal enclosure technique with an interval-based counterpart for the Dubins car model (35) with different domain size parameters R.

R	ρ	$\frac{\mathrm{vol}\{\mathscr{E}^{\mathrm{O}}_{x,k+1}\}}{\mathrm{vol}\{\mathscr{E}^{\mathrm{I}}_{x,k+1}\}}$	$\frac{\mathrm{vol}\{\mathscr{E}^{\mathrm{O}}_{x,k+1}\}}{\mathrm{vol}\{\mathscr{E}_{x,k}\}}$	$\frac{\mathrm{vol}\{[\mathbf{x}_{k+1}]\}}{\mathrm{vol}\{[\mathbf{x}_k]\}}$
2^{-2}	1.479	–	37.7316	9.3584
2^{-3}	0.350	18.5111	3.3160	3.7770
2^{-4}	0.085	1.9698	1.3835	2.1466
2^{-5}	0.021	1.1808	1.0857	1.5218
2^{-6}	$5.15\cdot10^{-3}$	1.0421	1.0208	1.2479
2^{-7}	$1.28\cdot10^{-3}$	1.0103	1.0052	1.1207
2^{-8}	$3.20\cdot10^{-4}$	1.0026	1.0013	1.0596
2^{-9}	$7.98\cdot10^{-5}$	1.0007	1.0004	1.0296
2^{-10}	$2.00\cdot10^{-5}$	1.0002	1.0001	1.0148

arithmetic-like enclosures (Krasnochtanova *et al.*, 2010).

4.2.2. Restricted planar three-body problem. The second example in this subsection is the restricted planar three-body problem in which a body with negligible mass $m_3 = 0$ moves under the influence of the gravitational fields of the two other masses m_1 and m_2. After normalizing the gravitational constant to the value of one, this system is described by a set of continuous-time equations of motion that represent the accelerations

$$\begin{aligned}
\dot{\mathbf{v}}^{(1)} &= \mathbf{f}_{v,1}\left(\mathbf{v}^{(1)},\mathbf{v}^{(2)},\mathbf{v}^{(3)}\right)\\
&= -m_2\frac{\mathbf{v}^{(1)}-\mathbf{v}^{(2)}}{\left\|\mathbf{v}^{(2)}-\mathbf{v}^{(1)}\right\|^3} - m_3\frac{\mathbf{v}^{(1)}-\mathbf{v}^{(3)}}{\left\|\mathbf{v}^{(3)}-\mathbf{v}^{(1)}\right\|^3},\\
\dot{\mathbf{v}}^{(2)} &= \mathbf{f}_{v,2}\left(\mathbf{v}^{(1)},\mathbf{v}^{(2)},\mathbf{v}^{(3)}\right)\\
&= -m_1\frac{\mathbf{v}^{(2)}-\mathbf{v}^{(1)}}{\left\|\mathbf{v}^{(2)}-\mathbf{v}^{(1)}\right\|^3} - m_3\frac{\mathbf{v}^{(2)}-\mathbf{v}^{(3)}}{\left\|(\mathbf{v}^{(3)}-\mathbf{v}^{(2)}\right\|^3},\\
\dot{\mathbf{v}}^{(3)} &= \mathbf{f}_{v,3}\left(\mathbf{v}^{(1)},\mathbf{v}^{(2)},\mathbf{v}^{(3)}\right)\\
&= -m_1\frac{\mathbf{v}^{(3)}-\mathbf{v}^{(1)}}{\left\|\mathbf{v}^{(3)}-\mathbf{v}^{(1)}\right\|^3} - m_2\frac{\mathbf{v}^{(3)}-\mathbf{v}^{(2)}}{\left\|\mathbf{v}^{(3)}-\mathbf{v}^{(2)}\right\|^3},
\end{aligned} \tag{38}$$

as well as the velocities

$$\dot{\boldsymbol{\chi}}^{(i)} = \mathbf{v}^{(i)}. \tag{39}$$

Here, $\boldsymbol{\chi}^{(i)} \in \mathbb{R}^2$ and $\mathbf{v}^{(i)} \in \mathbb{R}^2$ describe the position and velocity vectors, respectively, of each mass $i \in \{1,2,3\}$ according to Krishnaswami and Senapati (2019) as well as Musielak and Quarles (2014). For the numerical evaluation, this system model is discretized in time with the help of a symplectic Euler method (Hairer *et al.*, 2002) with the step size T resulting in

$$\begin{aligned}
\mathbf{v}^{(i)}_{k+1} &= \mathbf{v}^{(i)}_k + T\mathbf{f}_{v,i}\left(\mathbf{v}^{(1)}_k,\mathbf{v}^{(2)}_k,\mathbf{v}^{(3)}_k\right),\\
\boldsymbol{\chi}^{(i)}_{k+1} &= \boldsymbol{\chi}^{(i)}_k + T\mathbf{v}^{(i)}_{k+1},\ \ i\in\{1,2,3\},
\end{aligned} \tag{40}$$

which together represent the nonlinear function

$$\mathbf{x}_{k+1} = \begin{bmatrix}\boldsymbol{\chi}^T_{k+1} & \mathbf{v}^T_{k+1}\end{bmatrix}^T = \mathbf{f}(\mathbf{x}_k), \tag{41}$$

in which all positions and velocities are summarized in the stacked vectors

$$\begin{aligned}
\boldsymbol{\chi}_k &= \begin{bmatrix}\left(\boldsymbol{\chi}^{(1)}_k\right)^T & \left(\boldsymbol{\chi}^{(2)}_k\right)^T & \left(\boldsymbol{\chi}^{(3)}_k\right)^T\end{bmatrix}^T,\\
\mathbf{v}_k &= \begin{bmatrix}\left(\mathbf{v}^{(1)}_k\right)^T & \left(\mathbf{v}^{(2)}_k\right)^T & \left(\mathbf{v}^{(3)}_k\right)^T\end{bmatrix}^T,
\end{aligned} \tag{42}$$

with $\mathbf{x}_k = \begin{bmatrix}\boldsymbol{\chi}^T_k & \mathbf{v}^T_k\end{bmatrix}^T \in \mathbb{R}^{12}$. For the application of the proposed evaluation technique, the initial ellipsoid is defined by the midpoint vector

$$\begin{aligned}
\boldsymbol{\mu}_{x,k} &= \begin{bmatrix}-\alpha r & 0 & \beta r & 0 & \frac{r}{2}\frac{(m_1-m_2)}{m_1+m_2} & \frac{\sqrt{3}}{2}r & \boldsymbol{\mu}^T_{v,k}\end{bmatrix}^T,\\
\boldsymbol{\mu}_{v,k} &= \begin{bmatrix}0.1 & -0.1 & -0.1 & 0.1 & -0.1 & -0.1\end{bmatrix}^T,
\end{aligned} \tag{43}$$

with the initial distance $r = 100$ between the masses $m_1 = 10$ and $m_2 = 1$ with

$$\alpha = \frac{m_2}{m_1+m_2}, \quad \beta = \frac{m_1}{m_1+m_2}.$$

The point $\boldsymbol{\mu}_{x,k}$ corresponds to one of the Lagrangian points of the three-body system considered. Moreover, uncertainty is accounted for by the diagonal ellipsoid shape matrix

$$\mathbf{C}_{x,k} = R^2\cdot\left(\mathrm{diag}\left(\begin{bmatrix}\mu^2_{x,1,k} & \cdots & \mu^2_{x,12,k}\end{bmatrix}\right) + 10^{-8}\mathbf{I}\right), \tag{44}$$

whose entries depend on the squared entries of the midpoint vector with the parameter $R > 0$. The additive term $10^{-8}\mathbf{I}$ ensures small uncertainty in the positions that are zero in the midpoint vector $\boldsymbol{\mu}_{x,k}$. As for the Dubins car example, the alternative interval evaluation makes use of a tight axis-aligned box containing this ellipsoid.

The results of the evaluation are summarized in Table 3. They do not only confirm the superiority of the ellipsoidal enclosure technique in analogy to the previous example, but also indicate that the naive interval evaluation of the model (41) leads to a certain amount of pessimism if multiple dependencies on common interval arguments are not treated specifically, even for very small parameters R. However, this special treatment is not necessary for the ellipsoidal approach, because the centered form evaluation of the parameter ρ according to (25)–(26) possesses this property inherently.

Table 3. Comparison of the ellipsoidal enclosure technique with an interval-based counterpart for the three-mass system (41) with different domain size parameters R.

R	ρ	$\frac{\mathrm{vol}\{\mathscr{E}^{\mathrm{O}}_{x,k+1}\}}{\mathrm{vol}\{\mathscr{E}^{\mathrm{I}}_{x,k+1}\}}$	$\frac{\mathrm{vol}\{\mathscr{E}^{\mathrm{O}}_{x,k+1}\}}{\mathrm{vol}\{\mathscr{E}_{x,k}\}}$	$\frac{\mathrm{vol}\{[\mathbf{x}_{k+1}]\}}{\mathrm{vol}\{[\mathbf{x}_k]\}}$
2^{-2}	1.519	–	$6.514 \cdot 10^4$	$1.167 \cdot 10^6$
2^{-3}	0.197	117.51	8.5689	$1.139 \cdot 10^6$
2^{-4}	0.057	3.8836	1.9333	$1.133 \cdot 10^6$
2^{-5}	0.023	1.7043	1.3016	$1.167 \cdot 10^6$
2^{-6}	$9.94 \cdot 10^{-3}$	1.2694	1.1260	$1.131 \cdot 10^6$
2^{-7}	$4.72 \cdot 10^{-3}$	1.1197	1.0581	$1.131 \cdot 10^6$
2^{-8}	$2.30 \cdot 10^{-3}$	1.0567	1.0279	$1.131 \cdot 10^6$
2^{-9}	$1.14 \cdot 10^{-4}$	1.0276	1.0137	$1.131 \cdot 10^6$
2^{-10}	$5.63 \cdot 10^{-4}$	1.0136	1.0068	$1.131 \cdot 10^6$

Remark 5. Both the system models (35) and (41) are volume-preserving maps. Therefore, the ratio between the volume of the initial and predicted domains represents a measure for the arising overestimation in both the ellipsoidal and interval-based function evaluations. The preservation of the volume, regardless of the chosen step size T, can be verified by means of symbolic formula manipulation which proves that the determinants of the Jacobians of both functions $\mathbf{f}$ in (35) and (41) with respect to their input arguments are equal to one.

5. Application 2: Forecasting confidence ellipsoids

If uncertain parameters and state variables are represented in terms of stochastic probability distributions, they are often assumed to be normally distributed. As is well known from the design of Kalman filters (Kalman, 1960; Stengel, 1994), the assumption of a normal distribution of the resulting variables (both after state prediction and measurement-based innovation) is only preserved if the system models are linear in the variables to be estimated and if process and measurement noises influence the system in an additive way. If nonlinearities arise, Taylor linearization-based system approximations are often used to implement the so-called extended Kalman filter (EKF), which is based on the system's Jacobian at the latest estimate for the expectation of the probability density.

Therefore, this section proposes to use the ellipsoidal enclosure approach as a computationally cheap method to verify the admissibility of the aforementioned approximation of system models by a first-order Taylor linearization. If this is the case, the parameter ρ computed by means of Algorithm 1 is sufficiently close to zero so that the outer and inner ellipsoidal enclosures get close to the forecasted confidence bound that can be determined with the help of an EKF-based approximation in the prediction stage. In addition to forecasting the covariance ellipsoid, also further ellipsoidal level sets of the probability distribution can easily be investigated which correspond to a specific percentage of expected observations. For further approaches using uncertainty modeling by means of the so-called clouds, which are alternatively applicable to forecasting confidence bounds, the reader is referred to the technical report by Neumaier *et al*. (2007).

To make the proposed ellipsoidal enclosure approach applicable to the task of forecasting confidence ellipsoids, assume that the discrete-time one-step prediction of an uncertain state vector $\mathbf{x}_k$ follows the state equations

$$\mathbf{x}'_{k+1} = \mathbf{a}\left(\mathbf{x}'_k, \mathbf{w}_k\right), \tag{45}$$

where $\mathbf{w}_k$ is a stochastically distributed noise process. For the sake of compact notation, define further the augmented state vectors $\mathbf{x}_k = \begin{bmatrix}\mathbf{x}'^T_k & \mathbf{w}^T_k\end{bmatrix}^T$ and $\mathbf{x}_{k+1} = \begin{bmatrix}\mathbf{x}'^T_{k+1} & \mathbf{w}^T_k\end{bmatrix}^T$ so that (45) turns into

$$\mathbf{x}_{k+1} = \begin{bmatrix}\mathbf{a}\left(\mathbf{x}'_k, \mathbf{w}_k\right) \\ \mathbf{w}_k\end{bmatrix} =: \mathbf{f}\left(\mathbf{x}_k\right), \quad \mathbf{x}_k \in \mathbb{R}^n. \tag{46}$$

The theoretically exact solution of this state prediction step according to Eqn. (46), where $\mathbf{x}_k$ is characterized by its probability density $p_k(\mathbf{x}_k)$, is given by the evaluation of the multidimensional convolution integral (Papoulis, 1965; Rauh *et al*., 2009)

$$p_{k+1}\left(\mathbf{x}_{k+1}\right) = \int_{\mathbb{R}^n} p_k\left(\mathbf{x}_k\right) \cdot \delta\left(\mathbf{x}_{k+1} - \mathbf{f}\left(\mathbf{x}_k\right)\right) \mathrm{d}\mathbf{x}_k, \tag{47}$$

where $\delta(\cdot)$ is a multi-variate Dirac delta distribution. The corresponding integration needs to be carried out with care so that the support of the probability density $p_{k+1}(\mathbf{x}_{k+1})$ is restricted to the domain on which $\mathbf{x}_{k+1}$ is well defined.

Note that the predicted density $p_{k+1}(\mathbf{x}_{k+1})$ usually cannot be represented in closed analytic form if the system model under consideration is nonlinear. Then, starting with a Gaussian approximation of the prior knowledge $\mathbf{x}_k \sim \mathcal{N}(\boldsymbol{\mu}_k, \mathbf{C}_k)$, the predicted expectation and covariance are commonly approximated in terms of the EKF solution with

$$\boldsymbol{\mu}_{k+1} = \mathbf{f}(\boldsymbol{\mu}_k), \tag{48}$$

which is identical to the mapping of the ellipsoid center in the proposed approach, and

$$\mathbf{C}_{k+1} = \mathbf{A}_k \cdot \mathbf{C}_k \cdot \mathbf{A}_k^T, \tag{49}$$

respectively. In (49), $\mathbf{A}_k = \frac{\partial \mathbf{f}}{\partial \mathbf{x}_k}(\boldsymbol{\mu}_k)$ is the Jacobian of the model (46) evaluated at the mean $\boldsymbol{\mu}_k$ of the normally distributed approximation of the prior probability density. If the only information of interest is the probability

density $p_{k+1}\left(\mathbf{x}'_{k+1}\right)$ for a subspace of the augmented state vector $\mathbf{x}_{k+1}$, a marginalization of the combined state and disturbance density is performed by a projection onto the space $\mathbf{x}'_{k+1}$.

5.1. Illustrating example. To visualize the computational stages for forecasting confidence regions, consider the system model

$$\mathbf{x}_{k+1} = \begin{bmatrix} x_{k+1} \\ w_k \end{bmatrix} = \begin{bmatrix} 2x_k - 0.5x_k^3 + w_k \\ w_k \end{bmatrix}, \tag{50}$$

where the prior knowledge of x_k and w_k is assumed to be given by a Gaussian probability distribution with $\boldsymbol{\mu}_k = \mathbf{0}$ and $\mathbf{C}_k = R^2 \cdot \mathbf{I}$, $R > 0$.

Figure 4 shows the result of predicting the corresponding covariance bounds as the 1-standard deviation confidence region according to (45), on the basis of $2.5 \cdot 10^7$ random sampling points. Obviously, the mapping of all samples lying within the prior confidence ellipse (Fig. 4(a)) as well as that of all random samples (Fig. 4(b)) lead to distributions that deviate significantly from Gaussian densities. This effect can be detected easily if the new ellipsoidal enclosure approach is employed to forecast the inner and outer bounds of the covariance ellipse. Those ellipses are defined in such a way that the inequality (for a table of the probabilities for specific confidence levels of multi-variate normal distributions and their efficient computation, the reader is referred to Wang *et al*. (2015))

$$\mathrm{pr}\left(\mathbf{x}_{k+1} | \mathbf{x}_{k+1} \in \mathscr{E}^{\mathrm{I}}\right) \leq 0.3935 \leq \mathrm{pr}\left(\mathbf{x}_{k+1} | \mathbf{x}_{k+1} \in \mathscr{E}^{\mathrm{O}}\right) \tag{51}$$

holds, where $\mathrm{pr}(\cdot)$ denotes the cumulative probability over the specified domains.

After a marginalization of the Monte-Carlo sampling (retaining the first vector component of (50), where the true covariance bound then results in a percentage of 68.27%), the comparison of the inner and outer ellipsoid bounds with the EKF-based approximation clearly shows how the proposed approach can be used to detect that the EKF approximation is not reliable in this case (Fig. 4(c)). Note that this approximation is even independent of the nonlinearity in (50) due to the specific choice of the prior mean $\boldsymbol{\mu}_k$. As a countermeasure, nonlinear filtering techniques and probability density splitting approaches such as those of the PDSME (cf. Hanebeck *et al*., 2003; Rauh *et al*., 2009) could be used. From an interpretation point of view, the comparison of inner and outer ellipsoidal enclosures as a quality measure for the EKF-based approximation is much more intuitive than the Kullback–Leibler distance criterion published by Rauh *et al*. (2009).

Table 4 provides an overview of the quality increase of the EKF-based approximation for reducing ball diameters R.

Table 4. Ellipsoidal enclosures for the 1-standard deviation confidence interval of x_{k+1} in comparison with the EKF-based forecast in terms of the percentages of included sampling points.

	Ellipsoidal enclosures		
R	$\mathscr{E}^{\mathrm{I}}$	$\mathscr{E}^{\mathrm{O}}$	EKF
2^0	26.96%	98.80%	86.34%
2^{-1}	61.96%	82.02%	72.96%
2^{-2}	66.79%	71.43%	69.16%
2^{-4}	68.18%	68.46%	68.32%
2^{-6}	68.28%	68.30%	68.29%
2^{-8}	68.28%	68.28%	68.28%

5.2. Lithium-ion battery model. As a second nonacademic scenario, consider the electric equivalent circuit model for the dynamics of charging and discharging of Lithium-ion batteries represented by Fig. 5. This model can be extended according to Rauh *et al*. (2013) and Reuter *et al*. (2016) to perform a real-time capable estimation of aging parameters which represent (both reversible and irreversible) capacity loss, an increase in the internal battery resistance and changes in the time constants with respect to calendar life, cycling, and temperature effects.

Here, we restrict ourselves to a nominal battery model, representing the state of charge $\sigma(t)$ as well as the voltages $v_{\mathrm{TL}}(t)$ and $v_{\mathrm{TS}}(t)$ across two RC networks. Those subnetworks represent the time constants of electrochemical double layer effects, concentration polarization as well as electrochemical polarization. Moreover, the terminal current $i_{\mathrm{T}}(t)$ is a known control input applied to the battery, while the terminal voltage $v_{\mathrm{T}}(t)$ is employed as the measured system output.

Assuming a normalized state of charge $\sigma(t) \in [0\,;\,1]$, where $\sigma = 1$ corresponds to the fully charged battery and $\sigma = 0$ represents the completely discharged battery, a state of charge balancing is described by the integral relation

$$\dot{\sigma}(t) = -\frac{i_{\mathrm{T}}(t)}{C_{\mathrm{Bat}}}, \tag{52}$$

where C_{Bat} denotes the nominal capacity.

As described in detail by Chen and Rincon-Mora (2006), Erdinc *et al*. (2009) and Rauh *et al*. (2010), the open circuit voltage

$$\begin{aligned} v_{\mathrm{OC}}(\sigma(t)) = v_0 \cdot e^{v_1 \cdot \sigma(t)} + v_2 + v_3\sigma(t) \\ + v_4 \cdot \sigma^2(t) + v_5\sigma^3(t). \end{aligned} \tag{53}$$

is a function of the state of charge $\sigma(t)$. In addition, Ohmic voltage drops across the series resistance

$$R_{\mathrm{S}}(t) = R_{\mathrm{Sa}} \cdot e^{R_{\mathrm{Sb}} \cdot \sigma(t)} + R_{\mathrm{Sc}} \tag{54}$$

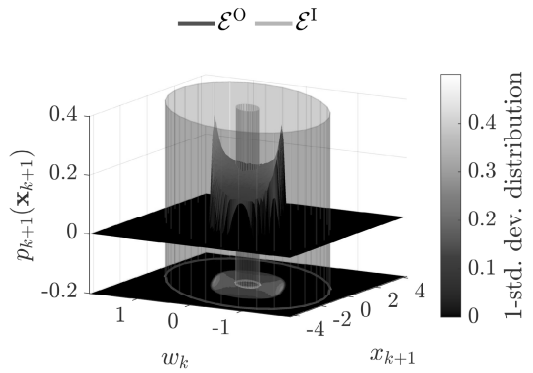

(a) Comparison of the inner and outer bounds of the covariance ellipsoid with the sampling points from the interior of the prior covariance ellipsoid.

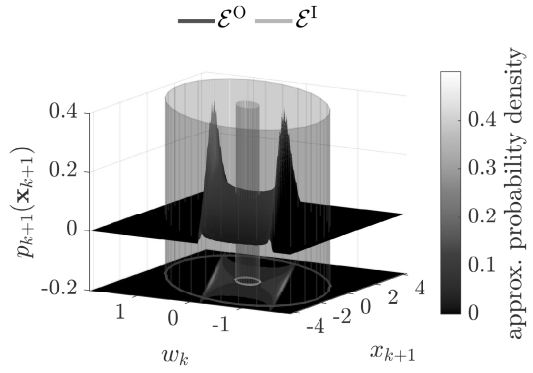

(b) Comparison of the inner and outer bounds of the covariance ellipsoid with all sampling points.

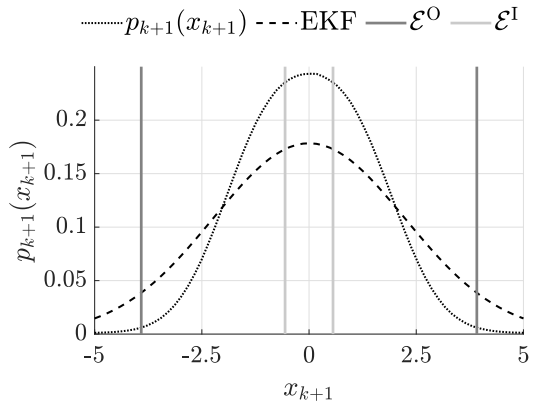

(c) Ellipsoidal enclosures for the 1-standard deviation confidence interval of x_{k+1} in comparison with the true and EKF-based probability densities.

Fig. 4. Simulation results for the example in Section 5.1.

and the aforementioned polarization effects (cf. Chen and Rincon-Mora, 2006; Erdinc *et al.*, 2009) lead to the expression

$$v_{\mathrm{T}}(t) = v_{\mathrm{OC}}(t) - i_{\mathrm{T}}(t) \cdot R_{\mathrm{S}}(t) - v_{\mathrm{TS}}(t) - v_{\mathrm{TL}}(t) \qquad (55)$$

for the terminal voltage, which can be obtained in a straightforward manner by means of Kirchhoff's voltage law.

Here, the electrochemical voltage drops over the previously mentioned RC subnetworks account for processes with short and large time constants (TS and TL, respectively), which may differ over several orders of magnitude. They are modeled by the ordinary differential equations

$$\dot{v}_{\mathrm{TS}}(t) = \frac{-v_{\mathrm{TS}}(t)}{C_{\mathrm{TS}}(t) \cdot R_{\mathrm{TS}}(t)} + \frac{i_{\mathrm{T}}(t)}{C_{\mathrm{TS}}(t)} \qquad (56)$$

and

$$\dot{v}_{\mathrm{TL}}(t) = \frac{-v_{\mathrm{TL}}(t)}{C_{\mathrm{TL}}(t) \cdot R_{\mathrm{TL}}(t)} + \frac{i_{\mathrm{T}}(t)}{C_{\mathrm{TL}}(t)}, \qquad (57)$$

with the state of charge dependent parameters

$$R_{\mathrm{TS}}(t) = R_{\mathrm{TSa}} \cdot e^{R_{\mathrm{TSb}} \cdot \sigma(t)} + R_{\mathrm{TSc}}, \qquad (58)$$

$$C_{\mathrm{TS}}(t) = C_{\mathrm{TSa}} \cdot e^{C_{\mathrm{TSb}} \cdot \sigma(t)} + C_{\mathrm{TSc}}, \qquad (59)$$

$$R_{\mathrm{TL}}(t) = R_{\mathrm{TLa}} \cdot e^{R_{\mathrm{TLb}} \cdot \sigma(t)} + R_{\mathrm{TLc}}, \qquad (60)$$

$$C_{\mathrm{TL}}(t) = C_{\mathrm{TLa}} \cdot e^{C_{\mathrm{TLb}} \cdot \sigma(t)} + C_{\mathrm{TLc}}. \qquad (61)$$

For the following numerical evaluation of this model, we make use of the experimental identification results of these parameters for a battery with the nominal capacity $C_{\mathrm{Bat}} = 3100\,\mathrm{mAh}$ that were published by Reuter *et al.* (2016). After the definition of the state vector

$$\mathbf{x}(t) := [\sigma(t)\ v_{\mathrm{TS}}(t)\ v_{\mathrm{TL}}(t)]^T, \qquad (62)$$

the ordinary differential equation model

$$\dot{\mathbf{x}}(t) = \mathbf{f}(\mathbf{x}(t), i_{\mathrm{T}}(t)), \qquad (63)$$

which comprises the individual state equations (52), (56), and (57), is discretized by an explicit Euler method with the step size $T = 1\,\mathrm{s}$ for the terminal current $i_{\mathrm{T}} = 1\,\mathrm{A}$. In addition, this algebraic model is augmented by the terminal voltage $v_{\mathrm{T}}(t_{k+1})$, so that a nonlinear model according to (46) with $n = 4$ is obtained. For the numerical evaluation, we choose

$$\boldsymbol{\mu}_k = \begin{bmatrix} \bar{\sigma} & 0.15 & 0.15 & 0 \end{bmatrix}^T, \qquad (64)$$

with the purely diagonal prior covariance matrix

$$\mathbf{C}_k = \begin{bmatrix} 1 \cdot 10^{-4} & 0 & 0 & 0 \\ 0 & 4 \cdot 10^{-8} & 0 & 0 \\ 0 & 0 & 4 \cdot 10^{-8} & 0 \\ 0 & 0 & 0 & 1 \cdot 10^{-6} \end{bmatrix}. \qquad (65)$$

In (64), the variable $\bar{\sigma}$ is introduced as a degree of freedom with which the influence of the actual state of charge of the battery on the system's nonlinearity can

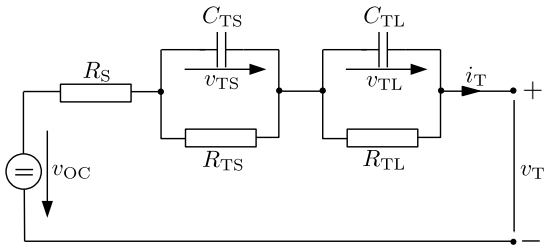

Fig. 5. Electric equivalent circuit of a battery.

be investigated in greater detail. All evaluations of this system model refer to 90% confidence intervals under the assumption of the above-stated normal distribution that is parameterized by (64) and (65).

Figures 6 and 7 provide a comparison of a Monte-Carlo sampling-based uncertainty evaluation for approximately $5 \cdot 10^4$ randomly chosen points as the depicted point clouds. Here, Fig. 6 has been evaluated for a relatively low state of charge $\bar{\sigma} = 0.25$, while Fig. 7 describes an almost fully charged battery with $\bar{\sigma} = 0.95$. It can be noticed that the computed outer ellipsoidal bounds (dark gray dashed lines) are very wide in the case of the low state of charge. This property reflects the large influence of nonlinearities for the corresponding operating point confirmed by Fig. 8(a), where the EKF-based 90% confidence bound obviously does not include all of the respective sampling points. This effect reduces significantly for larger states of charge; see also Figs. 8(b) and (c). Especially the latter graph highlights that not only the nonlinear, rapid drop in the open circuit voltage for low values of the state of charge plays a major role, but also all nonlinear dependencies within the time constants of both RC subnetworks need to be taken into consideration for an accurate state estimation.

Therefore, linearized estimation schemes tend to underestimate the true system behavior for small values of σ, while they can be expected to work well for a medium and sufficiently high state of charge. Due to the fact that excessively low values of the state of charge may lead to a rapid degradation of the battery, they need to be avoided by the application of battery management systems as well as by state of charge equalization schemes in battery packs in which numerous cells are electrically connected in series and parallel. Therefore, enhanced estimators, ranging from unscented Kalman filters (Julier *et al*., 2000) over more general nonlinear approaches (Hanebeck *et al*., 2003) to neural network implementations, should be preferred for small values of $\bar{\sigma}$. The distinction of whether a linear estimator suffices for a specific level of uncertainty (measured by the prior covariance) can directly be deduced from the absolute values of ρ that are computed with the help of Algorithm 1 proposed in this paper. This also holds if strategies for fault tolerant control or fault estimation are of interest; see the works of Farrera *et al*. (2020) and Mejdi *et al*. (2020) for further reading.

6. Conclusions and future work

In this paper, a computationally inexpensive ellipsoidal enclosure technique was presented which aims at enclosing the range of multi-dimensional functions both from the inside and outside. As illustrated by the presented examples, this approach not only can be employed in the frame of a set-valued context aiming at a verified reachability analysis and simulation, but it also provides valuable information on the accuracy of linear (resp. linearized) stochastic estimation schemes. For the latter aspect, forecasting confidence bounds during the prediction stage of a discrete-time system model was used as a representative benchmark in comparison with the well-known EKF solution.

Future work will employ this function evaluation technique for the implementation of set-valued simulation and state estimation procedures for nonlinear discrete-time as well as continuous-time systems for which the first developments were published by Rauh and Jaulin (2021) as well as Rauh *et al*. (2021a). Furthermore, it will be combined with the verification of stability as well as reachability properties. Moreover, domain splitting and merging techniques (similar to those employed by SIVIA in the work of Jaulin *et al*. (2001)) for classical interval representations of uncertainty will be incorporated for cases in which the pessimism, which can be forecasted rigorously by the absolute value of ρ, is unacceptably large. Finally, it is desired to generalize this approach to other set representations such as parallelepipeds.

References

Becis-Aubry, Y. (2020). Ellipsoidal constrained state estimation in presence of bounded disturbances, *Preprint*, `arxiv.org/pdf/2012.03267v1.pdf`.

Bünger, F. (2020). A Taylor model toolbox for solving ODEs implemented in MATLAB/INTLAB, *Journal of Computational and Applied Mathematics* **368**: 112511.

Bouissou, O., Chapoutot, A. and Djoudi, A. (2013). Enclosing temporal evolution of dynamical systems using numerical methods, *in* G. Brat *et al.* (Eds), *NASA Formal Methods*, Springer-Verlag, Berlin/Heidelberg, pp. 108–123.

Bourgois, A. and Jaulin, L. (2021). Interval centred form for proving stability of non-linear discrete-time systems, *in* T. Dang and S. Ratschan (Eds), *Symbolic-Numeric Methods for Reasoning About CPS and IoT*, Open Publishing Association, Den Haag, pp. 1–17.

Chapoutot, A. (2010). Interval slopes as a numerical abstract domain for floating-point variables, *in* R. Cousot and M.

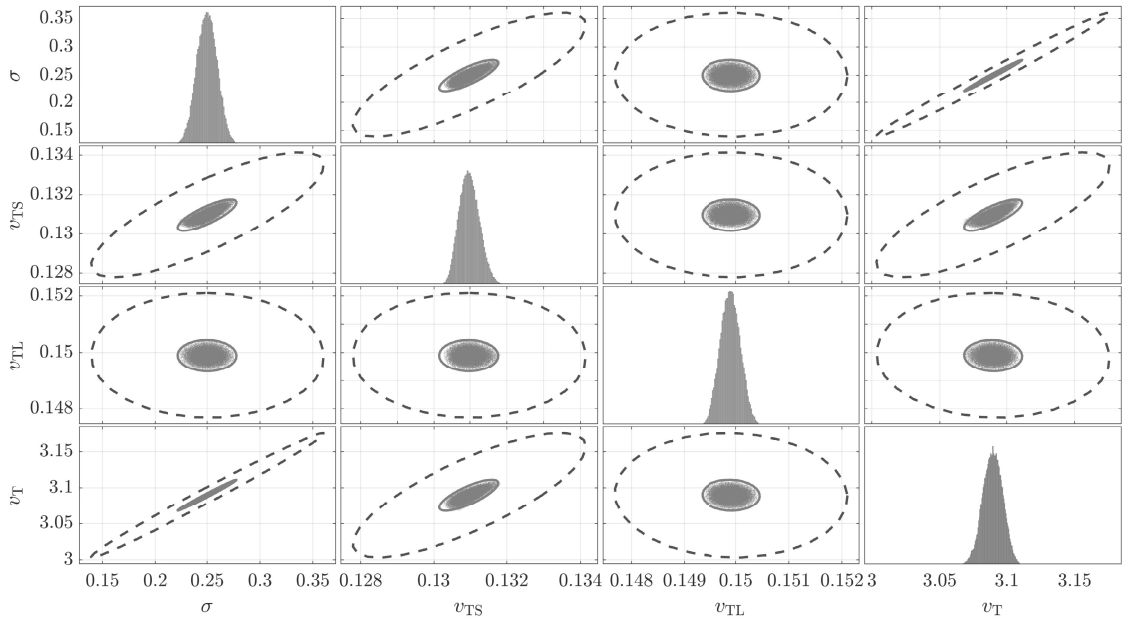

Fig. 6. Comparison of a Monte-Carlo sampling-based 90% confidence forecast with an EKF-based approximation (solid lines) and the outer ellipsoidal enclosure $\mathcal{E}^{\mathrm{O}}$ (dashed lines) for the mean value $\bar{\sigma} = 0.25$ of the state of charge.

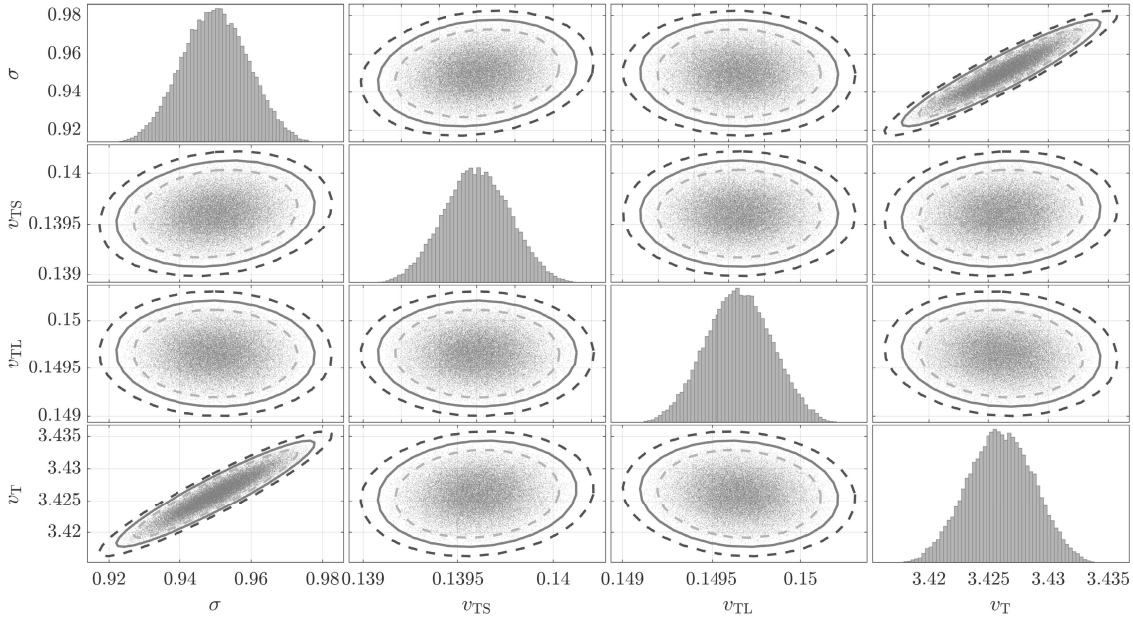

Fig. 7. Comparison of a Monte-Carlo sampling-based 90% confidence forecast with an EKF-based approximation (solid lines) and the outer and inner ellipsoidal enclosures $\mathcal{E}^{\mathrm{O}}$ and $\mathcal{E}^{\mathrm{I}}$ (dashed lines) for the mean value $\bar{\sigma} = 0.95$ of the state of charge.

Martel (Eds), *Static Analysis. SAS 2010*, Lecture Notes in Computer Science, Vol. 6337, Springer, Berlin/Heidelberg, pp. 184–200.

Chen, M. and Rincon-Mora, G. (2006). Accurate electrical battery model capable of predicting runtime and I-V performance, *IEEE Transactions on Energy Conversion* **21**(2): 504–511.

Cornelius, H. and Lohner, R. (1984). Computing the range of values of real functions with accuracy higher than second order, *Computing* **33**(3–4): 331–347.

de Berg, M., Cheong, O., van Kreveld, M. and Overmars, M. (2008). *Computational Geometry: Algorithms and Applications*, 3rd Edn, Springer, Berlin/Heidelberg.

Erdinc, O., Vural, B. and Uzunoglu, M. (2009). A dynamic Lithium-ion battery model considering the effects of temperature and capacity fading, *International Conference on Clean Electrical Power, Capri, Italy*, pp. 383–386.

Černý, M. (2012). Goffin's algorithm for zonotopes, *Kybernetika* **48**(5): 890–906.

Farrera, B., López-Estrada, F.-R., Chadli, M., Valencia-Palomo, G. and Gómez-Peñate, S. (2020). Distributed fault estimation of multi-agent systems using a proportional-integral observer: A leader-following application, *International Journal of Applied Mathematics and Computer Science* **30**(3): 551–560, DOI: 10.34768/amcs-2020-0040.

Goubault, E., Mullier, O., Putot, S. and Kieffer, M. (2014). Inner approximated reachability analysis, *17th International Conference on Hybrid Systems: Computation and Control, Berlin, Germany*, pp. 163–172.

Griewank, A. (2000). *Evaluating Derivatives: Principles and Techniques of Algorithmic Differentiation*, SIAM, Philadelphia.

Hairer, E., Lubich, C. and Wanner, G. (2002). *Geometric Numerical Integration: Structure-Preserving Algorithms for Ordinary Differential Equations*, Springer, Berlin/Heidelberg.

Halder, A. (2018). On the parameterized computation of minimum volume outer ellipsoid of Minkowski sum of ellipsoids, *IEEE Conference on Decision and Control (CDC), Miami Beach, USA,* pp. 4040–4045.

Hanebeck, U.D., Briechle, K. and Rauh, A. (2003). Progressive Bayes: A new framework for nonlinear state estimation, *in* B.V. Dasarathy (Ed.), *Multisensor, Multisource Information Fusion: Architectures, Algorithms, and Applications 2003*, International Society for Optics and Photonics, Bellingham, pp. 256–267.

Hoefkens, J. (2001). *Rigorous Numerical Analysis with High-Order Taylor Models*, PhD thesis, Michigan State University, East Lansing, `https://groups.nscl.msu.edu/nscl_library/Thesis/Hoefkens,%20Jens.pdf`.

Houska, B., Villanueva, M. and Chachuat, B. (2015). Stable set-valued integration of nonlinear dynamic systems using affine set-parameterizations, *SIAM Journal on Numerical Analysis* **53**(5): 2307–2328.

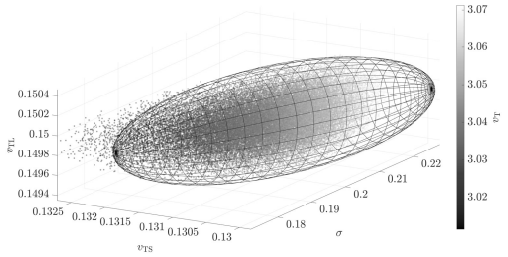

(a) Comparison of the EKF-based confidence approximation with the 90% point cloud for $\bar{\sigma} = 0.20$.

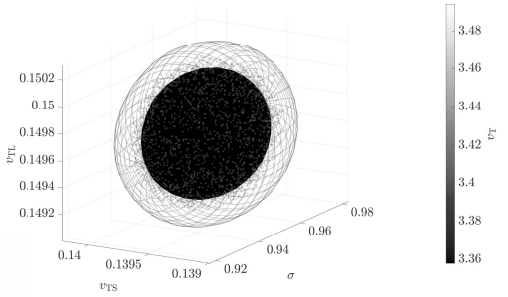

(b) Comparison of the outer and inner confidence ellipsoids with the 90% point cloud for $\bar{\sigma} = 0.95$.

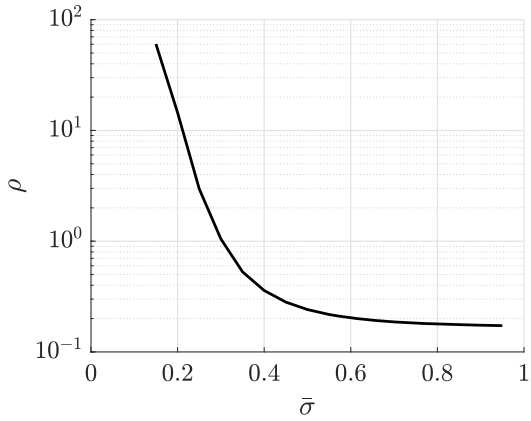

(c) Dependence between the excess width ρ and the average state of charge $\bar{\sigma}$.

Fig. 8. Visualization of the 90% confidence regions of the Lithium-ion battery model in Fig. 5.

Jambawalikar, S. and Kumar, P. (2008). A note on approximate minimum volume enclosing ellipsoid of ellipsoids, *International Conference on Computational Sciences and Its Applications, Perugia, Italy*, pp. 478–487.

Jaulin, L., Kieffer, M., Didrit, O. and Walter, É. (2001). *Applied Interval Analysis*, Springer-Verlag, London.

John, F. (1948). Extremum problems with inequalities as subsidiary conditions, *Studies and Essays Presented to R. Courant on his 60th Birthday*, Interscience Publishers, New York, pp. 187–204.

Julier, S., Uhlmann, J. and Durrant-Whyte, H. (2000). A new

approach for the nonlinear transformation of means and covariances in filters and estimators, *IEEE Transactions on Automatic Control* **45**(3): 477–482.

Kalman, R. (1960). A new approach to linear filtering and prediction problems, *Transaction of the ASME: Journal of Basic Engineering* **82**(Series D): 35–45.

Krasnochtanova, I., Rauh, A., Kletting, M., Aschemann, H., Hofer, E.P. and Schoop, K.-M. (2010). Interval methods as a simulation tool for the dynamics of biological wastewater treatment processes with parameter uncertainties, *Applied Mathematical Modeling* **34**(3): 744–762.

Krishnaswami, G. and Senapati, H. (2019). An introduction to the classical three-body problem: From periodic solutions to instabilities and chaos, *Reson* 24: 87–114, DOI: 10.1007/s12045-019-0760-1.

Kühn, W. (1999). Rigorous error bounds for the initial value problem based on defect estimation, *Technical report*, `http://www.decatur.de/personal/papers/defect.zip`.

Kurzhanskii, A.B. and Vályi, I. (1997). *Ellipsoidal Calculus for Estimation and Control*, Birkhäuser, Boston.

Kurzhanskiy, A. and Varaiya, P. (2006). Ellipsoidal Toolbox (ET), *Proceedings of the 45th IEEE Conference on Decision and Control, San Diego, USA,* pp. 1498–1503.

Makino, K. and Berz, M. (2004). Suppression of the wrapping effect by Taylor model-based validated integrators, *Technical Report MSU HEP 40910*, Michigan State University, East Lansing.

Mayer, G. (2017). *Interval Analysis and Automatic Result Verification*, De Gruyter, Berlin/Boston.

Mejdi, S., Messaoud, A. and Ben Abdennour, R. (2020). Fault tolerant multicontrollers for nonlinear systems: A real validation on a chemical process, *International Journal of Applied Mathematics and Computer Science* **30**(1): 61–74, DOI: 10.34768/amcs-2020-0005.

Moore, R. (1966). *Interval Arithmetic*, Prentice-Hall, Englewood Cliffs.

Moore, R., Kearfott, R. and Cloud, M. (2009). *Introduction to Interval Analysis*, SIAM, Philadelphia.

Musielak, Z.E. and Quarles, B. (2014). The three-body problem, *Reports on Progress in Physics* **77**(6): 065901.

Neumaier, A., Fuchs, M., Dolejsi, E., Csendes, T., Dombi, J. and Banhelyi, B. (2007). Application of clouds for modeling uncertainties in robust space system design, *Technical Report 05-5201*, European Space Agency, Paris, `http://www.esa.int/gsp/ACT/doc/ARI/ARI%20Study%20Report/ACT-RPT-INF-ARI-055201-Clouds.pdf`.

Papoulis, A. (1965). *Probability, Random Variables, and Stochastic Processes*, McGraw-Hill, Tokyo.

Rauh, A., Bourgois, A. and Jaulin, L. (2021a). Ellipsoidal enclosure techniques for a verified simulation of initial value problems for ordinary differential equations, *5th International Conference on Control, Automation and Diagnosis (ICCAD'21), Grenoble, France*, (accepted for publication).

Rauh, A., Bourgois, A. and Jaulin, L. (2021b). Union and intersection operators for thick ellipsoid state enclosures: Application to bounded-error discrete-time state observer design, *Algorithms* **14**(3): 88.

Rauh, A., Briechle, K. and Hanebeck, U.D. (2009). Nonlinear measurement update and prediction: Prior density splitting mixture estimator, *IEEE International Conference on Control Applications CCA 2009, St. Petersburg, Russia*, pp. 1421–1426.

Rauh, A., Butt, S.S. and Aschemann, H. (2013). Nonlinear state observers and extended Kalman filters for battery systems, *International Journal of Applied Mathematics and Computer Science* **23**(3): 539–556, DOI: 10.2478/amcs-2013-0041.

Rauh, A. and Jaulin, L. (2021). A novel thick ellipsoid approach for verified outer and inner state enclosures of discrete-time dynamic systems, *19th IFAC Symposium on System Identification: Learning Models for Decision and Control*, online.

Rauh, A., Kletting, M., Aschemann, H. and Hofer, E.P. (2007). Reduction of overestimation in interval arithmetic simulation of biological wastewater treatment processes, *Journal of Computational and Applied Mathematics* **199**(2): 207–212.

Rauh, A., Weitschat, R. and Aschemann, H. (2010). Modellgestützter Beobachterentwurf zur Betriebszustands- und Alterungserkennung für Lithium-Ionen-Batterien, *VDI-Berichte 2105: Innovative Fahrzeugantriebe 2010 Die Vielfalt der Mobilität: Vom Verbrenner bis zum E-Motor: 7. VDI-Tagung Innovative Fahrzeugantriebe, Dresden, Germany*, pp. 377–382.

Reuter, J., Mank, E., Aschemann, H. and Rauh, A. (2016). Battery state observation and condition monitoring using online minimization, *21st Internatioanl Conference on Methods and Models in Automation and Robotics, Międzyzdroje, Poland*, pp. 1223–1228.

Romig, S., Jaulin, L. and Rauh, A. (2019). Using interval analysis to compute the invariant set of a nonlinear closed-loop control system, *Algorithms* **12**(12): 262.

Stengel, R. (1994). *Optimal Control and Estimation*, Dover Publications, New York.

Tarbouriech, S., Garcia, G., Gomes da Silva, J. and Queinnec, I. (2011). *Stability and Stabilization of Linear Systems With Saturating Actuators*, Springer-Verlag, London.

Tóth, B. and Csendes, T. (2005). Empirical investigation of the convergence speed of inclusion functions in a global optimization context, *Reliable Computing* **11**: 253–273.

Villanueva, M., Houska, B. and Chachuat, B. (2015). Unified framework for the propagation of continuous-time enclosures for parametric nonlinear ODEs, *Journal of Global Optimization* **62**(3): 575–613.

Wang, B., Shi, W. and Miao, Z. (2015). Confidence analysis of standard deviational ellipse and its extension into higher dimensional Euclidean space, *PLOS ONE* **10**(3): 1–17.

Yildirim, E.A. (2006). On the minimum volume covering ellipsoid of ellipsoids, *SIAM Journal on Optimization* **17**(3): 621–641.

Andreas Rauh was born in Munich, Germany, in 1977. He received his diploma degree in electrical engineering and information technology from Technische Universität München, Germany, in 2001, his PhD (Dr.-Ing.) from the University of Ulm, Germany, in 2008, and his habilitation (Dr.-Ing. habil.) in measurement technology and automatic control from the University of Rostock, Germany, in 2017. He has published more than 170 articles and chapters in edited books, international conferences and peer-reviewed journals, with the focus on modeling, control, as well as state and parameter estimation for systems with stochastic and set-valued uncertainties. Since 2008 he has been a member of the IEEE 1788 Working Group for the Standardization of Interval Arithmetic.

Luc Jaulin was born in Nevers, France, in 1967. He received his PhD degree in automatic control from the University of Orsay, France, in 1993 and his *Habilitation à Diriger des Recherches* degree in 2000. He is currently a full professor of robotics at ENSTA Bretagne (Ecole Nationale Supérieure de Techniques Avancées), France. He focuses his research on underwater robotics using interval methods and constraint propagation in team ROBEX—ROBotics for EXploration of Lab-STICC. He is a co-author of more than 250 papers in international journals and congresses. He received the Moore prize in 2012 for his work on localization and map building of underwater robots using interval constraint propagation.

Received: 9 December 2020
Revised: 12 April 2021
Re-revised: 25 May 2021
Accepted: 28 May 2021